International Journal of Electrical and Computer Engineering (IJECE)
Vol. 16, No. 3, June 2026, pp. 1249~1260
ISSN: 2088-8708, DOI: 10.11591/ijece.v16i3.pp1249-1260

Sub-X-band reconfigurable antenna network with graphene slots

Hassna Agoumi[1], Seddik Bri[2], Youssef El Amraoui[3], Adil Saadi[1]
[1]Modeling, Information Processing and Control Systems (MIPCS), National Graduate School of Arts and Crafts, Moulay Ismail University, Meknes, Morocco
[2]Intelligent Electrical Systems, Materials and Components, High School of Technology, Moulay Ismail University, Meknes, Morocco
[3]Laboratory of Condensed Matter and Interdisciplinary Science (LaMCScI), Faculty of Science, Mohammed V University, Rabat, Morocco

Article Info

Article history:

Received Aug 29, 2025
Revised Mar 27, 2026
Accepted Apr 26, 2026

Keywords:

Bandwidth enhancement
Gain improvement
Graphene-based antenna
Hexagonal patch antenna
Planar antenna array
Reconfigurable antenna
Sub-x-band

ABSTRACT

This paper presents the design and analysis of a graphene-slotted hexagonal microstrip patch antenna and its extension to a compact 4×4 planar array operating in the sub-X-band. The objective of this work is to demonstrate that graphene-based electrical reconfigurability can be extended from a single antenna element to an array configuration while improving radiation performance. The proposed antenna integrates graphene slots etched into the radiating patch, where reconfigurability is achieved by electrically tuning the graphene conductivity through an external gate voltage V_g. The single antenna operates around 9.4 GHz with an impedance bandwidth of 400 MHz and a peak gain of 6 dB. The design is then extended to a 4×4 array with an inter-element spacing of approximately 1.2 wavelengths. The array operates in the 9–10 GHz range, provides a bandwidth of 380 MHz, and achieves a maximum gain of 13.08 dB. The results confirm that graphene-enabled reconfigurability can be preserved at the array level without increasing structural complexity.

Corresponding Author:

Hassna Agoumi
Modeling, Information Processing and Control Systems (MIPCS), National Graduate School of Arts and Crafts, Moulay Ismail University
15290 ENSAM, Meknes 50500, Morocco
Email: h.agoumi@edu.umi.ac.ma.

1. INTRODUCTION

Microstrip patch antennas are extensively employed in modern wireless communication systems due to their compact size, low profile, ease of fabrication, and compatibility with planar and printed circuit technologies [1]. They are commonly used in applications such as automotive radar, satellite communications, and wireless systems. It is in the fields of high-resolution radar, military communications, and advanced wireless applications that the X-band finds all its interest among the microwave bands, due to its balance between resolution and propagation.

In addition to increasing the transmission rate, multiple-input-multiple-output (MIMO) technologies improve the reliability of systems and their robustness against interference [1]. Compact reconfigurable radar and communication platforms ideally operate in the 9-10 GHz band. However, to fully exploit optimal MIMO performance, the radiating elements must combine efficiency and flexibility.

The high conductivity of copper patch antennas does not compensate for two main limitations in advanced applications: confined reconfigurability and spectral rigidity [2]. Graphene, a promising two-dimensional material, effectively addresses these limitations thanks to its surface conductivity, which is adjustable by gate voltage, which ensures significantly improved electrical performance [3].

Graphene enables frequency reconfigurability in radiating structures without relying on active components such as positive intrinsic negative (PIN) diodes, microelectromechanical systems (MEMS), or transistors [4]. Patch antennas incorporating graphene slots enable local impedance tuning and controlled activation of radiating zones [5]. Previous research highlights the superior performance of graphene-based antennas in terms of bandwidth, directivity, and adaptability [6]. Broadband architectures, adaptive MIMO systems, cognitive antennas, and intelligent radars are among the primary beneficiaries of this spectral flexibility [7]. Furthermore, graphene's atomic-scale thickness facilitates the realization of compact devices while maintaining high performance [8]. Nevertheless, most existing studies on graphene-based antennas remain limited to single-element configurations or theoretical analyses, with only a few works addressing practical reconfigurable implementations. Recent studies have demonstrated frequency reconfigurable radio frequency (RF) and microwave antennas based on graphene, exploiting gate-voltage control through surface conductivity or quantum capacitance [9], [10]. Other works have explored beam or radiation reconfiguration using graphene-based concepts at sub-6 GHz or higher frequency regimes [11], while comprehensive investigations of graphene-based antenna arrays are mainly reported outside the conventional microwave Sub-X-band or remain at a conceptual level [12]. As a result, the behavior of compact, reconfigurable graphene antenna arrays operating in the sub-X-band has yet to be thoroughly investigated.

To address the limited investigation of compact graphene-based antenna arrays in the sub-X-band, we present the design, simulation, and analysis of a single microstrip patch antenna and its extension to a 4×4 reconfigurable array incorporating graphene-based slots, optimized for 9–10 GHz operation. Unlike conventional approaches relying on PIN diodes or MEMS switches, the proposed method achieves frequency agility through gate-voltage-controlled surface conductivity modulation, dynamically controlling impedance matching and surface current distribution. The contributions of this work include the implementation of a passive graphene-slot reconfiguration mechanism within a scalable microwave array architecture and the validation of its electromagnetic performance. Thanks to graphene, the proposed structure outperforms the conventional copper design in terms of bandwidth, gain, and directivity. These improvements validate novelty and the practical interest of reconfigurable networks for adaptive microwave antenna structures.

This work extends the theoretical framework of microstrip patch antennas by incorporating a material-driven reconfiguration mechanism based on the tunable surface conductivity of graphene. It shows that variations in graphene conductivity effectively modify the boundary conditions and the effective electrical length of the radiating element, thereby influencing the resonant behavior. This establishes a direct relationship between material properties and electromagnetic response. Consequently, the proposed approach refines conventional impedance matching and resonance models for adaptive antenna arrays.

2. RESEARCH METHOD

This section presents a methodology for designing a reconfigurable graphene-based antenna. It describes the transition from a single radiating element to a 4×4 array operating in the sub-X-band (9-10 GHz). The antenna is modeled using full-wave electromagnetic simulations with CST Microwave Studio. Reconfigurability is achieved by integrating graphene slots, which are represented by a tunable surface impedance controlled through a gate voltage V_g. The array configuration is then optimized in terms of inter-element spacing to evaluate the impact of graphene tunability on antenna performance.

2.1. Graphene conductivity model

The surface conductivity of graphene, denoted by σ_s, arises from both interband and intraband electronic transitions. However, in the gigahertz frequency range, the intraband contribution dominates, while the interband contribution can be neglected. Under this assumption, the graphene surface conductivity can be expressed using the intraband Kubo formulation, as shown in (1) [13].

$$\sigma_s = \frac{-je^2K_BT}{\pi\hbar^2(\omega - j\tau^{-1})}\left[\frac{\mu_C}{K_BT} + 2ln\left(e^{\frac{-\mu_C}{K_BT}} + 1\right)\right] \quad (1)$$

Where ω is the angular frequency in (rad.s^{-1}), τ is the relaxation time in (s), μ_c is the chemical potential of graphene in (eV), T is the absolute temperature in (K), e is the electron charge in (C), $\hbar$ is the reduced Planck constant in (J.s), and k_B is the Boltzmann constant in (J.K^{-1}).

As described by (1), the graphene surface conductivity is mainly governed by three key parameters: the relaxation time τ, the temperature T, and the chemical potential μ_c, which represents the doping level of graphene. The chemical potential can be controlled by an external gate-voltage denoted by V_g, allowing the graphene sheet to exhibit either high or low surface conductivity. As a result, this model accurately reproduces the high (ON state) and low (OFF state) conductivity of graphene.

2.2. Electrical tunability with gate voltage

The use of an applied gate voltage V_g enables dynamic control of the chemical potential μ_c of graphene and provides active control of its surface conductivity. The relationship between gate-voltage V_g and chemical potential μ_c is given by (2) [14].

$$V_g = \frac{e\mu_c{}^2 h}{\pi\hbar^2 v_f{}^2 \varepsilon_0 \varepsilon_r} \quad (2)$$

Where V_g is the applied gate-voltage in (V), e is the electron charge in (C), μ_c is the chemical potential of graphene in (eV), h is the substrate thickness in (mm), $\hbar$ is the reduced Planck constant in (J.s), v_f is the Fermi velocity in graphene in (m.s^{-1}), ε_r is the relative permittivity of the substrate, and ε_0 is the permittivity of free space in (F.m^{-1}). According to (2), an increased chemical potential resulting from a higher gate-voltage improves the surface conductivity. This mechanism enables reconfigurable electromagnetic properties.

2.3. Structural geometry of the proposed antenna

The hexagonal-shaped microstrip patch is implemented on an epoxy FR4 substrate with a relative permittivity of 4.3 and a thickness of 1.6 mm. The main design parameters of this patch antenna are presented in Table 1. The proposed antenna is an irregular hexagonal microstrip patch. Its geometry is defined by the overall patch length Lp, the effective vertical dimension $Lp1$, and the lateral patch length $Lp2$.

The cavity transmission line model from [15] provides an initial approximation of the effective electrical length of the radiating element $Lp1$, denoted by L_{eff} (effective patch length), as expressed in (3).

$$L_{eff} = \frac{c}{2f_r\sqrt{\varepsilon_{eff}}} \quad (3)$$

Where c is the speed of light in (m.s^{-1}), f_r is the resonant frequency in (GHz), and ε_{eff} is the effective dielectric constant of the substrate.

The remaining dimensions, namely the main patch length Lp and the lateral length $Lp2$, are derived from the geometric constraints of the irregular hexagonal shape. For irregular geometries, closed-form analytical expressions have limited accuracy. Therefore, the parameters are adjusted through full-wave electromagnetic simulations to achieve the required resonance and impedance matching conditions [16].

The modification of the surface current distribution, induced by the insertion of slots in the patch, optimizes the impedance matching. Dynamic variation of the effective electrical length, without alteration of the physical dimensions, is ensured by the conductivity of the graphene. Figure 1 illustrates the antenna geometry, where Figure 1(a) shows the reference patch and Figure 1(b) presents the graphene-slotted configuration. The optimized dimensional parameters of the ground plane, substrate, patch, feed line, and slots are summarized in Table 2.

Table 1. Essential parameters of the proposed antenna

Parameter	Value
Resonant frequency, f_r (GHz)	9.46
Relative permittivity of the substrate (ε_r)	4.3
Substrate thickness, h (mm)	1.6
Antenna input impedance, R_{in} (Ω)	50

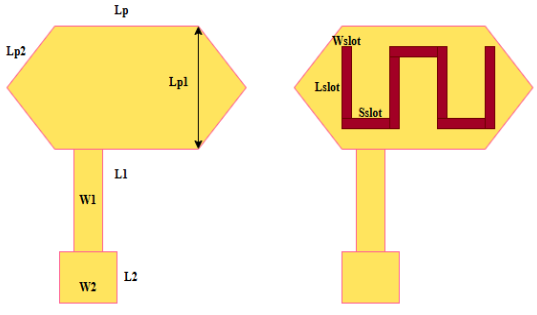

Figure 1. Geometry of the proposed hexagonal patch antenna: (a) reference element and (b) graphene-slotted configuration

Table 2. Optimized geometric parameters of the proposed graphene-slotted patch antenna

Parameter	Optimized value in (mm)
Main patch length *Lp*	10.20
Effective vertical patch dimension *Lp*1	8.80
lateral patch length *Lp*2	8.50
Feed line length *L*1	6.80
Feed line width *W*1	2.00
Impedance Matching length *L*2	2.90
Impedance Matching width *W*2	3.00
Slot width *Wslot*	0.75
Slot length *Lslot*	8.75
Inter slot spacing *Sslot*	3.75

Following finalization of the antenna design, the surface current distribution is evaluated. An essential step for assessing how the graphene slots influence radiative performance and reconfigurability. In particular, surface current evolution highlights the role of graphene in modifying effective current paths and resonance characteristics. Accordingly, the following section examines the surface current distribution of the proposed antenna in both the ON and OFF states of the graphene slots.

2.4. Surface current distribution in ON and OFF states

Frequency reconfigurability is achieved by controlling the current surface distribution through the integrated graphene slots, which are strategically placed in regions with high current density. The system is based on graphene switching: in the ON state, its reduced impedance allows the current to pass through the slots; in the OFF state, the increased impedance cuts off this conduction, which shifts the effective electrical length of the patch and modifies its resonance. This mechanism enables precise tuning of the antenna's electromagnetic performance.

The surface impedance values corresponding to the ON and OFF states are calculated using (4) to (9) [17].

$$\eta = \frac{\varepsilon_0 \varepsilon_r V_g}{de} \tag{4}$$

$$\mu_c = \hbar v_f \sqrt{\eta\pi} \tag{5}$$

$$\tau_s = \frac{4\hbar^2 \rho_m v_f {V_{ph}}^2}{\sqrt{\eta\pi}\, K_B T D^2} \tag{6}$$

$$\tau_L = \frac{\mu_L \hbar \sqrt{\eta\pi}}{e v_f} \tag{7}$$

$$\frac{1}{\tau} = \frac{1}{\tau_L} + \frac{1}{\tau_s} \tag{8}$$

$$Z_s = \frac{1}{\sigma(\omega, \mu_c, \tau, T)} = \frac{j\pi\hbar^2(\omega\tau_L\tau_S - j(\tau_L+\tau_S))}{e^2(\tau_L\tau_S)\left[\mu_c + 2K_B T ln\left(e^{\frac{-\mu_c}{K_B T}}+1\right)\right]} \tag{9}$$

Where η is the carrier density in (m^{-2}), $\rho_m = 7.6 \times 10^{-7}\ Kg/m^2$ is the two-dimensional mass density of graphene, $v_{ph} = 2.1 \times 10^4\ m/s$ is the sound velocity of longitudinal acoustic phonons in graphene, D is the deformation potential in (eV), μ_L is the electron mobility in ($m^2.(V.s)^{-1}$), τ_L is due to long-range scattering mechanisms such as defects and in purities, and τ_s is due to short-range scattering mechanisms such as phonon and carrier interactions.

The values of surface impedance Z_s for the ON and OFF states are obtained from (9). In this study, these two states are achieved without the use of discrete RF switches. In CST, graphene is modeled as a tunable ohmic surface impedance controlled by the gate voltage V_g. High and low conductivity corresponds to the ON and OFF states, respectively. Consequently, the resulting frequency responses arise directly from the electrical modulation of the graphene properties. Figure 2 illustrates the simulated surface current distribution of the graphene-slotted patch antenna at the resonant frequency, and the corresponding impedance parameters are summarized in Table 3.

The surface current distribution at 9.46 GHz exhibits strong confinement and effective guidance along the hexagonal patch. This behavior clearly highlights the structural influence of the graphene slots. As

explicitly shown in Figure 2(a), When graphene is in the ON state, it exhibits a low surface impedance $Z_s = 6.09 + j0.5\ \Omega$. The high surface current density observed in the slots under this condition, validates the improvement of electromagnetic conduction. Consequently, the radiation efficiency improves, the resonance mechanism strengthens, and the bandwidth widens. The resulting current distribution is both uniform and appropriately oriented, demonstrating coherent interaction among the patch's distinct regions.

Conversely, Figure 2(b) demonstrates that in the OFF state, graphene's high surface impedance $Z_s = 1552 + j1.8\ \Omega$, electrically deactivates the slots and renders their radiative contribution negligible. Surface currents then concentrate on the main patch, weakening coupling and reducing bandwidth enhancement. These distributions provide physical insight into the radiation mechanism, validating the electromagnetic consistency of the simulations.

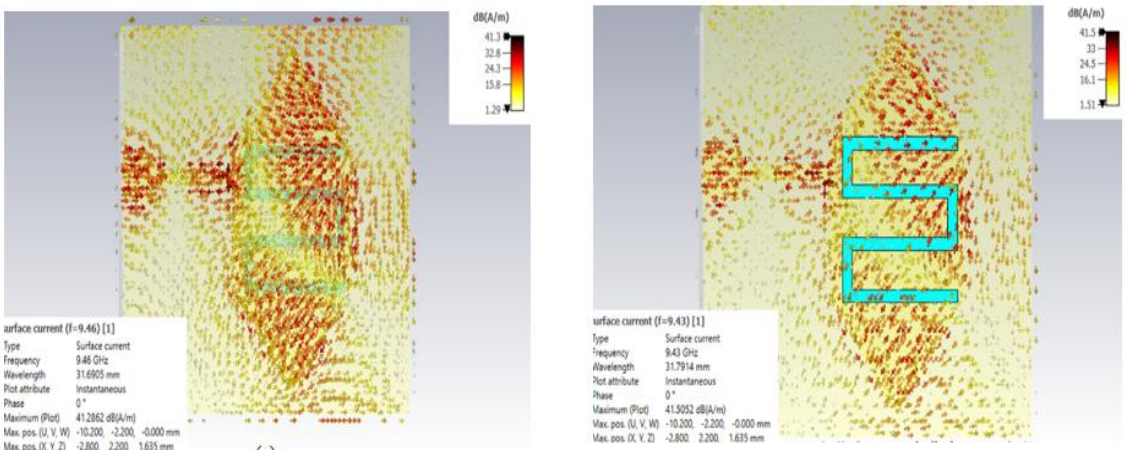

(a) (b)

Figure 2. Surface current distribution of the graphene-slotted patch antenna at 9.46 GHz: (a) graphene ON state and (b) graphene OFF state

Table 3. Selected parameters of the graphene surface impedance for ON and OFF states

State	ON state	OFF state
Gate-voltage V_g (V)	21	0.05
Temperature T (k)	300	300
Carrier concentration η (m^{-2})	5.8×10^{17}	6×10^{14}
Graphene Surface impedance Zs(Ω/□)	$6.09 + j0.5$	$1552 + j1.8$

2.5. Modeling of the 4×4 hexagonal patch array

The 4×4 array topology was selected as the optimal compromise between performance and practicality. Smaller arrays lack sufficient aperture and gain in the X-band, while larger arrays introduce excessive size, stronger coupling, and greater feeding complexity. The adopted layout thus combines compactness and symmetry with stable radiation, controlled side lobes, and enhanced bandwidth, making it ideal for intelligent antenna systems.

Inter-element spacing is a key design parameter in array antennas. Excessive separation generates grating lobes, whereas insufficient spacing widens the main beam and increases mutual coupling. Very tight spacing also complicates feeding network integration. Hence, the inter element distance must be optimized to balance radiation performance with practical feasibility [18].

An inter-element spacing of 1.2λ, selected along the x and y axes, serves to create the proposed 4×4 array by replication of the optimized single radiating element. Increased directivity and gain, with a controlled size: this spacing ensures compatibility with radar and wireless systems.

A waveguide port, positioned at the input of the structure, ensures proper excitation of the array. The frequency response, the gain and the radiation behavior of the array are evaluated using full-wave electromagnetic simulations. Figure 3 presents the final layout of the optimized 4×4 antenna array.

All electromagnetic simulations are performed using the time-domain solver. The antenna is excited via a 50 Ω waveguide port, and open (radiation) boundary conditions are applied.to emulate the propagation in free space. An adaptive mesh refinement strategy is employed to ensure numerical convergence. The

antenna performance is evaluated in terms of reflection coefficient (S11), impedance bandwidth, realized gain, and radiation patterns.

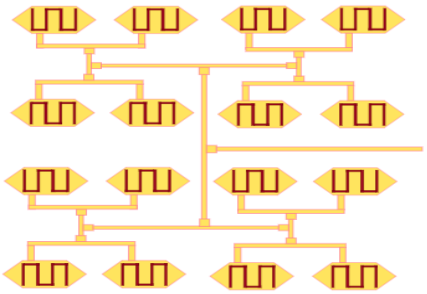

Figure 3. Corporate feeding network architecture of the proposed 4×4 hexagonal patch antenna for uniform power distribution

Fabrication feasibility of the proposed antenna is supported by recent studies in literature. It has been demonstrated that graphene can be synthesized by chemical vapor deposition (CVD), transferred onto dielectric substrates, and patterned using lithography techniques suitable for RF applications. However fabrication tolerances may affect the resonant frequency, impedance matching, and gain [19]. Furthermore, the performance of graphene-based antennas has been shown to depend on material properties such as surface conductivity, post-transfer uniformity, and metal-graphene contact resistance, yet it remains robust under realistic fabrication conditions [20]. Experimental fabrication and characterization therefore constitute natural directions for future work.

3. RESULTS AND DISCUSSION

In this section, the simulated results of the proposed antennas are presented and discussed. These results are obtained from full-wave electromagnetic simulations conducted under validated and realistic modeling conditions. They include the reflection coefficient, gain, and radiation patterns for both the single hexagonal patch element and the 4×4 array, considering the graphene OFF and ON configurations.

3.1. Single hexagonal patch antenna

Figure 4 shows the reflection coefficient S11 of the proposed antenna. Graphene slot integration improves impedance matching and increases the operating bandwidth compared with the copper reference. Electrical biasing induces a frequency shift of about 30 MHz between the ON and OFF states, confirming frequency reconfigurability. The ON states 400 MHz bandwidth serves as confirmation of graphene's dual functionality: improving bandwidth and enabling frequency reconfigurability at the same time.

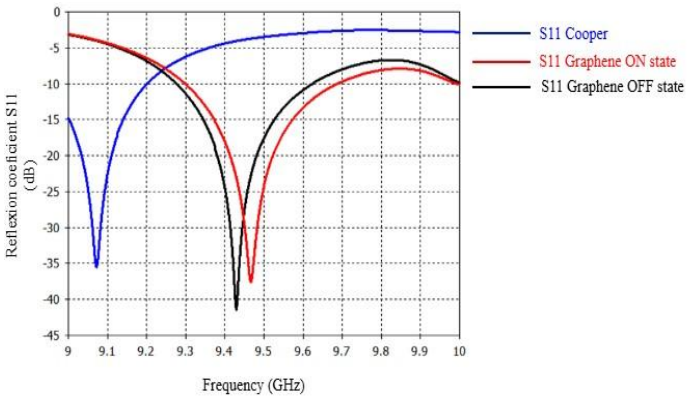

Figure 4. Comparison between the S_{11} responses of the copper reference and the graphene-based antenna in ON and OFF state

Figure 5 illustrates the gain achieved by the copper and graphene-based antenna configurations, alongside that of a conventional copper antenna. Thanks to graphene slot integration, both peak gain and gain stability are improved across the operating band. The OFF state provides higher gain levels over a wider frequency range, while the ON state achieves the highest gain performance, reaching approximately 6 dB. The findings show that graphene provides improved radiation performance while simultaneously enabling electrical gain control.

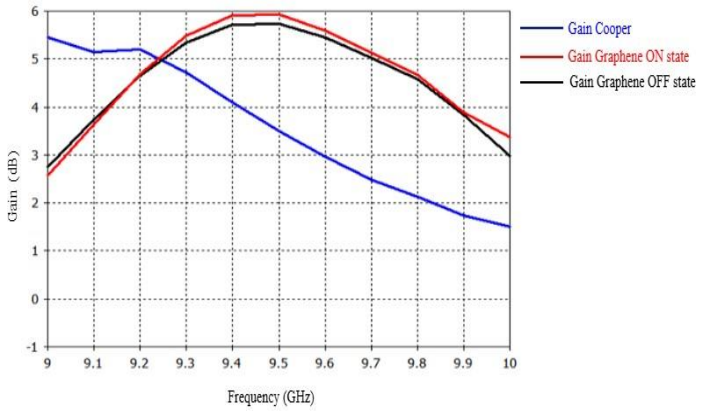

Figure 5. Gain for the copper-antenna and the graphene-based antenna in ON and OFF states

The simulated H-plane far-field radiation patterns of the copper and graphene-based antenna configurations are reported in Figure 6. Specifically, Figure 6(a) illustrates the radiation pattern of the conventional copper antenna, which serves as a baseline. The graphene-based antenna offers higher directivity while preserving a beamwidth comparable to that of the copper reference, as clearly demonstrated by the patterns for the OFF and ON states in Figure 6(b) and Figure 6(c), respectively. The slight modification of radiation characteristics under electrical biasing demonstrates that frequency reconfigurability is achieved without significantly distorting the beam. The findings confirm that graphene integration improves directivity while preserving pattern stability.

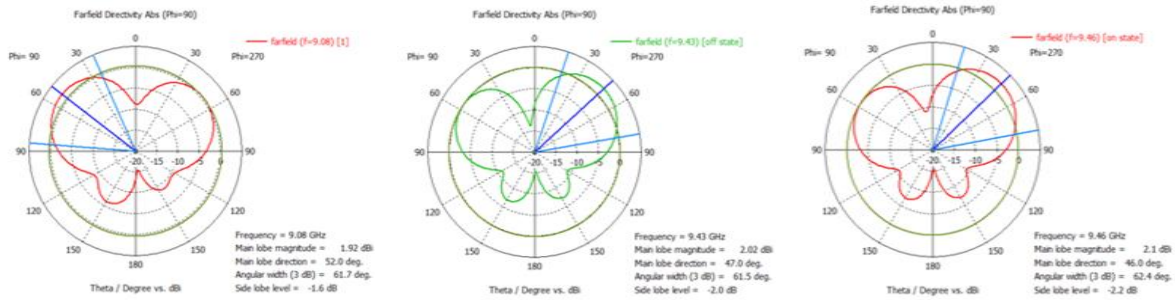

(a) (b) (c)

Figure 6. Comparison of the radiation diagrams (H-plane) obtained by simulation for the copper antenna and the graphene antenna in its two operating states: (a) conventional copper antenna as a reference, (b) graphene antenna in the OFF state, and (c) graphene antenna in the ON state

3.2. 4×4 hexagonal patch array

Figure 7 shows the reflection coefficient S11 of the proposed graphene-based 4×4 array. A wide operating bandwidth is attributed to the presence of multiple resonant modes. A bandwidth of approximately 380 MHz is attained in the ON state, representing a 26% increase relative to the 300 MHz observed in the OFF state. The two states exhibit a frequency shift of approximately 80 MHz, thereby confirming the array's reconfigurable behavior. These findings confirm that integrating graphene enhances bandwidth and provides tunable operation at the array level.

The gain performance of the 4×4 array is depicted in Figure 8. Around 9.25 GHz, the OFF state delivers a peak gain of about 11.8 dB. By contrast, activating the ON state enhances the gain at higher frequencies, with a maximum value of 13.08 dB recorded at 9.9 GHz. These findings confirm the efficacy of the proposed array architecture.

Figure 9 shows the far-field radiation pattern of the 4×4 array at 9.9 GHz. The main beam is directed close to broadside and provides a high directional gain of about 11.5 dB. The sidelobe levels remain limited to approximately –6.7 dB, which is acceptable for a compact planar array. This behavior reflects the trade-off between gain enhancement and side-lobe control associated with the chosen inter-element spacing of about 1.2 wavelengths. Overall, the results confirm that the selected array configuration achieves high gain while maintaining controlled radiation characteristics.

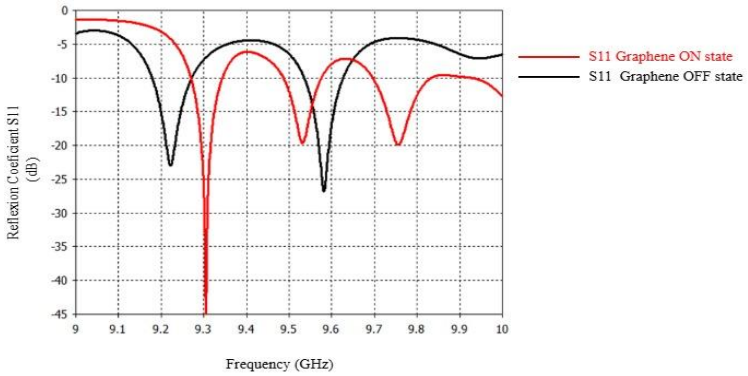

Figure 7. Reflection coefficient S11 of the 4×4 hexagonal patch antenna array (graphene ON/OFF states)

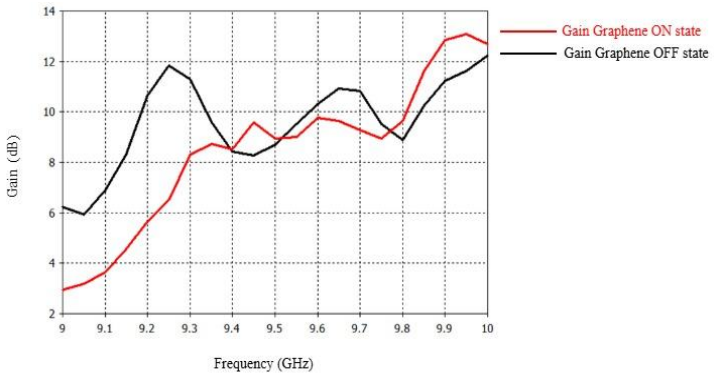

Figure 8. Frequency dependent gain of the 4×4 hexagonal patch antenna array (graphene ON/OFF state)

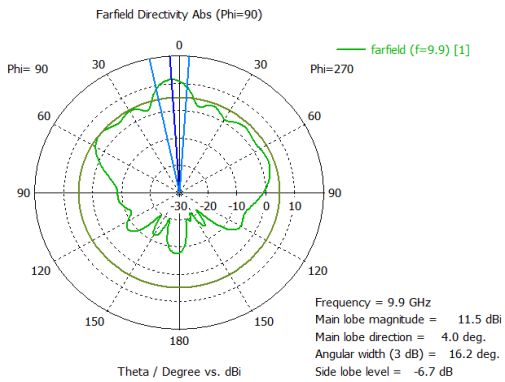

Figure 9. Directivity pattern of the 4×4 hexagonal patch antenna array at 9.9 GHz

The gain improvement obtained with the 4×4 network is more than twice that of the single element, without altering the impedance bandwidth. Moreover, the array response is characterized by multiple resonant modes, which contribute to improved frequency coverage in the sub-X-band. These results demonstrate that the chosen array configuration provides an effective compromise between gain, bandwidth, array efficiency, and sidelobe performance.

Unlike the majority of existing studies, which are primarily restricted to single reconfigurable antenna elements, the present work demonstrates the extension of graphene tunability to a compact 4×4 planar array, while preserving reconfigurability at the array level and enabling gain enhancement without the use of discrete RF switches or complex biasing networks. This approach represents a scalable and practically viable solution for graphene reconfigurable antenna arrays operating in the sub-X-band.

3.3. Performance comparison with previous studies

3.3.1. Single hexagonal patch antenna

Table 4 compares the proposed antenna with recent state-of-the-art reconfigurable designs. While active antennas using PIN diodes achieve wide bandwidths or multi-band operation [21]–[23], they require complex biasing networks and consume DC power. In contrast, the proposed hexagonal patch antenna with graphene slots provides passive frequency selectivity centered at 9.42 GHz within the sub-X-band. It achieves a peak gain of 6 dB, comparable to the 6.7 dB of [21] but with significantly lower implementation complexity and zero DC power consumption. Although its impedance bandwidth (400 MHz) is narrower than some active designs, this selectivity is advantageous for interference rejection in fixed-frequency X-band applications, making it ideal for compact, low-cost, and energy-efficient wireless systems.

Table 4. Comparison of the proposed single hexagonal patch antenna with reported reconfigurable antennas

Reference	Technology	Resonant Frequency (GHz)	Impedance Bandwidth (MHz)	Peak gain (dB)	Reconfigurability	Implementation complexity
[21]	Circular fractal patch with PIN diodes	10.22	670	6.7	active	High (diode + bias lines
[22]	Patch antenna with two PIN diodes	2.44 2.47	30	4.8	active	Medium (2 PIN+ micro-controller)
[23]	UWB fractal antenna with plus-shaped parasitic elements and 2 PIN diodes	4.7, 7.92, 10	6570	5.83	active	Medium PIN diodes
This work	Hexagonal patch antenna with graphene slots	9.42 9.43	400	6	passive	Low (no active elements)

3.3.2. 4×4 hexagonal patch array

A comparison between the proposed 4×4 hexagonal graphene-slotted patch array and recent multi-element antenna arrays is presented in Table 5. A peak gain of 13.08 dB is achieved at 9.30 GHz within the sub-X-band by the proposed design, which simultaneously offers two distinct advantages. The design integrates 16 radiating elements in a compact hexagonal layout, far more than the 4 elements used in typical high-gain arrays. The improvement in aperture efficiency and beamforming is directly attributed to the higher element density. While narrower than many ultra-wideband antennas, the 380 MHz bandwidth results from a conscious trade-off to maintain frequency selectivity. Graphene slots enable passive frequency reconfigurability, thereby removing the need for active components and lowering both system complexity and DC power consumption. This design attributes equal weight to architectural simplicity, gain, element density, and frequency relevance, thus avoiding any exclusive focus on a single performance criterion.

Table 5. Comparison of the proposed 4×4 hexagonal patch array with reported multi element antenna arrays

Reference	Technology	Resonant Frequency (GHz)	Impedance Bandwidth (MHz)	Peak gain (dB)	Number of elements
[24]	Dual-band cascaded patch antenna array with CSRR	3.1 4.4	210	5.69	16
[25]	Dual-band dipole array antenna with fan-beam characteristics	9.08 9.66	580	11.30	4
[26]	Multiport patch antenna for 2-D beam synthesis	27.5 28.5	1000	9	8
[27]	Dual circularly polarized patch array with orthogonal feed	10	132	12.87	4
This work	Graphene-slotted 4×4 hexagonal patch antenna array	9.30 9.55 9.78	380	13.08	16

4. CONCLUSION

While conventional copper designs are characterized by limited adaptability, the integration of graphene slots in the proposed hexagonal patch antenna offers improved impedance matching, extended bandwidth, and higher gain. The single-element configuration, operating in the sub-X-band (9–10 GHz), exhibits a bandwidth of 400 MHz and a peak gain of 6 dB. When extended to a 4×4 planar array, the graphene-based structure delivers a bandwidth of 380 MHz and a gain of approximately 13 dB, all the while maintaining a compact and lightweight footprint. The main limitations are the reliance on simulations, simplified graphene modeling, and the absence of experimental validation and practical biasing. Future research will focus on antenna fabrication and measurements, as well as on the investigation of real-time electrical tunability of graphene parameters using dynamic biasing schemes.

ACKNOWLEDGMENTS

The authors would like to thank their institution for providing the facilities necessary to conduct this research.

FUNDING INFORMATION

The authors declare that no funding was received for this work.

AUTHOR CONTRIBUTIONS STATEMENT

This journal uses the Contributor Roles Taxonomy (CRediT) to recognize individual author contributions, reduce authorship disputes, and facilitate collaboration.

Name of Author	C	M	So	Va	Fo	I	R	D	O	E	Vi	Su	P	Fu
Hassna Agoumi	✓	✓	✓	✓	✓	✓		✓	✓	✓	✓			
Seddik Bri	✓	✓		✓	✓		✓			✓		✓		
Youssef El Amraoui				✓								✓	✓	
Adil Saadi	✓	✓		✓						✓		✓		

C : **C**onceptualization
M : **M**ethodology
So : **So**ftware
Va : **Va**lidation
Fo : **Fo**rmal analysis
I : **I**nvestigation
R : **R**esources
D : **D**ata Curation
O : Writing - **O**riginal Draft
E : Writing - Review & **E**diting
Vi : **Vi**sualization
Su : **Su**pervision
P : **P**roject administration
Fu : **Fu**nding acquisition

CONFLICT OF INTEREST STATEMENT

The authors declare that they have no conflict of interest.

DATA AVAILABILITY

The authors confirm that the data supporting the findings of this study are available within the article.

REFERENCES

[1] S. M. Nimmagadda, S. F. Ahamed, and V. K. Padarti, "A comprehensive review on massive MIMO systems for 6G and beyond networks using ML and DL techniques," *Wireless Personal Communications*, vol. 144, no. 1–2, pp. 275–312, Sep. 2025, doi: 10.1007/s11277-025-11850-z.

[2] A. Sakkas *et al.*, "A frequency selective reconfigurable antenna for wireless applications in the S and C bands," *Sensors (Basel, Switzerland)*, vol. 23, no. 21, p. 8912, Nov. 2023, doi: 10.3390/s23218912.

[3] I. Eddine Lamri *et al.*, "Design and development of a graphene-based reconfigurable patch antenna array for THz applications," *Frequenz*, vol. 77, no. 3–4, pp. 219–228, Jul. 2023, doi: 10.1515/freq-2022-0051.

[4] A. G. Alharbi and V. Sorathiya, "Ultra-wideband graphene-based micro sized circular patch shaped yagi like MIMO antenna for terahertz wireless communication," *Electronics (Switzerland)*, vol. 11, no. 9, p. 1305, Apr. 2022, doi: 10.3390/electronics11091305.

[5] K. Aliqab, M. Alsharari, V. Sorathiya, and A. Armghan, "A numerical investigation of graphene-based hilbert shaped multi-band MIMO antenna for the terahertz spectrum applications," *Sensors*, vol. 23, no. 1, p. 37, Dec. 2023, doi: 10.3390/s23010037.

[6] B. Ahammed, T. Karim, and M. A. Alim, "Investigation of graphene functionalized multi-band MIMO antenna with enhanced isolation with high gain for THz applications," *Discover Electronics*, vol. 2, no. 1, p. 11, Mar. 2025, doi: 10.1007/s44291-025-

00050-5.
[7] M. Mashayekhi, P. Kabiri, A. S. Nooramin, and M. Soleimani, "A reconfigurable graphene patch antenna inverse design at terahertz frequencies," *Scientific Reports*, vol. 13, no. 1, p. 8369, May 2023, doi: 10.1038/s41598-023-35036-4.
[8] Z. Guo *et al.*, "Room-temperature terahertz detector based on monolayer graphene integrated with an asymmetric bowtie antenna," *Photonics*, vol. 10, no. 5, p. 576, May 2023, doi: 10.3390/photonics10050576.
[9] A. A. Megahed, M. E. Mousa, A. J. A. Al-Gburi, and R. H. Elabd, "Graphene-based frequency-reconfigurable slot antenna with gain enhancement using integrated metasurface for terahertz applications," *Optical and Quantum Electronics*, vol. 57, no. 10, p. 555, Sep. 2025, doi: 10.1007/s11082-025-08464-x.
[10] X. Wang, L. Wu, H. Chen, W. Wang, and Z. Liu, "Frequency reconfigurable microstrip patch antenna based on graphene film," *Electronics (Switzerland)*, vol. 12, no. 10, p. 2307, May 2023, doi: 10.3390/electronics12102307.
[11] S. Dash, C. Psomas, and I. Krikidis, "Graphene-based beam-reconfigurable liquid antenna for 5G mmWave wireless systems," *Frontiers in Communications and Networks*, vol. 6, p. 1560311, Mar. 2025, doi: 10.3389/frcmn.2025.1560311.
[12] A. Kumar, M. Aljaidi, I. Kansal, K. Alshammari, G. Gupta, and S. M. Alenezi, "Recent trends in reconfigurable antennas for modern wireless communication: A comprehensive review," *International Journal of Antennas and Propagation*, vol. 2024, no. 8816812, p. 24, Nov. 2024, doi: 10.1155/ijap/8816812.
[13] N. Kiani, F. Tavakkol Hamedani, and P. Rezaei, "Graphene-based quad port MIMO reconfigurable antennas for THz applications," *Silicon*, vol. 16, no. 9, pp. 3641–3655, Jun. 2024, doi: 10.1007/s12633-024-02939-4.
[14] E. A. Aydın, "3D printed graphene-based bowtie microstrip antenna design and analysis for ultra-wideband applications," *Polymers*, vol. 13, no. 21, p. 3724, Oct. 2021, doi: 10.3390/polym13213724.
[15] D. Yang, A. Das, S. D. Campbell, and D. H. Werner, "Harmonic engineering of antennas with time periodic substrate permittivity," *Physical Review Applied*, vol. 23, no. 2, p. 24008, Feb. 2025, doi: 10.1103/PhysRevApplied.23.024008.
[16] M. Biswas, S. Ghosh, S. Dey, K. Patra, and B. Gupta, "Design and analysis of irregular hexagonal patch antenna using multiport network model (MNM)," *International Journal of RF and Microwave Computer-Aided Engineering*, vol. 2024, no. 1, p. 8343100, Jul. 2024, doi: 10.1155/2024/8343100.
[17] H. M. Marhoon and N. Qasem, "Simulation and optimization of tuneable microstrip patch antenna for fifth-generation applications based on graphene," *International Journal of Electrical and Computer Engineering*, vol. 10, no. 5, pp. 5546–5558, Oct. 2020, doi: 10.11591/IJECE.V10I5.PP5546-5558.
[18] P. Wu, Y. H. Liu, Z. Q. Zhao, and Q. H. Liu, "Sparse antenna array design methodologies–A review," *Journal of Electronic Science and Technology*, vol. 22, no. 3, p. 100276, Sep. 2024, doi: 10.1016/j.jnlest.2024.100276.
[19] M. A. Haque *et al.*, "Graphene based terahertz MIMO antenna with machine learning regression for 6G communications," *Scientific reports*, vol. 16, no. 1, p. 3900, Jan. 2026, doi: 10.1038/s41598-025-32487-9.
[20] H. J. Hwang, S. Y. Kim, S. K. Lee, and B. H. Lee, "Reconfigurable single-layer graphene radio frequency antenna device capable of changing resonant frequency," *Nanomaterials*, vol. 13, no. 7, p. 1203, Mar. 2023, doi: 10.3390/nano13071203.
[21] I. Masroor, J. A. Ansari, A. Pandey, and P. K. Mishra, "Design and analysis of multiband fractal reconfigurable antenna using PIN diodes for smart wireless communications," *Progress in Electromagnetics Research C*, vol. 120, pp. 209–222, Jun. 2022, doi: 10.2528/PIERC22041402.
[22] T. Nguyen-Dinh, T. Dao-Duc, D. Nguyen-Quoc, H. Tran-Huy, and N. Hussain, "A method to design polarization reconfigurable antenna with simple switching mechanism and compact size characteristics," *Scientific Reports*, vol. 15, no. 1, p. 13387, Apr. 2025, doi: 10.1038/s41598-025-97908-1.
[23] M. Marzouk *et al.*, "Low profile reconfigurable UWB fractal antenna enhanced by parasitic elements for wireless applications," *Progress in Electromagnetics Research Letters*, vol. 126, pp. 37–48, May 2025, doi: 10.2528/PIERL25040402.
[24] M. Chandrasekhar and K. Kumarnaik, "Design a dual-band with CSRR cascaded patch antenna array for wireless communications," *Progress in Electromagnetic Research C*, vol. 149, pp. 155–163, Nov. 2024, doi: 10.2528/PIERC24090602.
[25] R. Barzegari, C.Ghobadi, J. Nourinia, and M. Shokri , "A dual-band dipole array antenna with fan beam characteristics for C- and X-band applications," *IEEE Access*, vol. 11, pp. 67330–67338, 2023, doi: 10.1109/ACCESS.2023.3291417.
[26] S. Rezaeeahvanouee and Y. Tousi, "Analytical study of configurable multiport patch antenna for 2-D beam synthesis," *IEEE Antennas and Wireless Propagation Letters*, vol. 24, no. 5, pp. 1109–1113, 2025, doi: 10.1109/LAWP.2025.3526522.
[27] D. Das, Md. F. Hossain, and Md. A. Hossain, "A simple feed orthogonal excitation X-band dual circular polarized microstrip patch array antenna," *International Journal of Electrical and Computer Engineering*, vol. 14, no. 2, pp. 1604–1615, Apr. 2024, doi: 10.11591/ijece.v14i2.pp1604-1615.

BIOGRAPHIES OF AUTHORS

Hassna Agoumi received her master's degree in telecommunications and microwave devices from Sidi Mohamed Ben Abdellah University, Fes, Morocco, in 2011 and her bachelor's degree in electrical engineering from Moulay Ismail University, Meknes, Morocco, in 2005.She is currently a Ph.D. student in electrical engineering at Moulay Ismail University, Meknes, Morocco. She can be contacted at email: h.agoumi@edu.umi.ac.ma.

Seddik Bri Professor at the High School of Technology (ESTM), Moulay Ismail University, Meknes, Morocco. His research interests include material characterization, patch antenna design, microwave applications, and security in communication systems. He has contributed to several studies on antenna design and microwave devices. He can be contacted at e mail: s.bri@umi.ac.ma.

Youssef El Amraoui received his Bachelor's and master's degrees in physics from Mohammed V University, Rabat, Morocco, in 1989 and 1990 respectively, and his Ph.D. in Physics from Moulay Ismail University, Meknes, Morocco, in 1998. He is currently a Professor at Mohammed V University, Rabat, Morocco. His research focuses on the theoretical study of phase transitions in disordered systems. He can be contacted at e mail: yelamraoui@hotmail.com.

Adil Saadi was born in Morocco in 1970. He received his Ph.D. from Ibnou Tofail University, Kenitra, Morocco, in 2003. He is currently a Professor at Moulay Ismail University, Meknes, Morocco. His research interests include microwave biomedical applications such as hyperthermia and cancer detection. He is currently developing microwave components using transverse section method (TSM) for industrial microwave applications. He can be contacted at e mail: a.saadi@umi.ac.ma.